DOI: 10.1002/ejic.200500983

Facile and Selected-Control Synthesis of β-MnO_2 Nanorods and Their Magnetic Properties

Guangli Wang,[a] Bo Tang,*[a] Linhai Zhuo,[a] Jiechao Ge,[a] and Mei Xue[a]

Keywords: β-Manganese dioxide / Nanostructures / Hydrothermal synthesis / Magnetic properties

Single crystal β-MnO_2 nanorods were successfully synthesized employing a facile in-situ redox precipitation hydrothermal process. The effects of various experimental conditions on the morphology of the products were investigated. The mechanism of formation of the nanorods was investigated and discussed based on the experimental results. The magnetic measurement of the nanorods with a diameter of 25–40 nm and a length of 240–440 nm indicates that the Néel magnetic transition temperature is about 6 K higher than that of the bulk β-MnO_2 crystal.

1. Introduction

One-dimensional (1D) nanocrystals such as nanorods, nanowires, and nanotubes have been the focus of considerable interest.[1–3] As a consequence of their low dimensionality and quantum confinement effect, they can show unique electronic, optical, and magnetic properties that are anomalous when compared to the bulk materials.[4–7] Manganese dioxide can form many kinds of polymorph, such as α-, β-, γ-, and δ-types, each offering distinctive properties and applications. Applications include as molecular sieves, ion sieves, in catalysis, as cathode materials for secondary rechargeable batteries, and as new magnetic materials.[8–12] Bach et al.[13] have especially pointed out that the electrochemical properties of MnO_2 strongly depend on parameters such as powder morphology, crystalline structure, and bulk density. One-dimensional nanostructures are the smallest structures known for the efficient transport of electrons, and they may provide the possibility of detecting the theoretical operating limits of a lithium battery.[14–15] MnO_2 also possesses an interesting magnetic structure.[16–20] To date we have found nothing in the literature on the magnetic properties of nanosized MnO_2. Therefore, development of a controllable synthesis method for one-dimensional MnO_2 nanostructures was deemed very important to be able to explore their novel properties as well as examine potential applications for MnO_2. Much effort has been put into preparing nanocrystalline MnO_2 with different crystallographic forms; such as nanorod-shaped and nanofibrous α- and Tokorokite-type MnO_2,[21] β-MnO_2 nanorods,[22] γ-MnO_2 nanowires,[23] and δ-MnO_2 nanofibers.[24] Although Li et al. have reported on the hydrothermal synthesis of α-MnO_2 nanowires and β-MnO_2 nanorods by oxidizing $MnSO_4$ with $KMnO_4$ or $K_2S_2O_8$, respectively,[22] the control of both morphology and the phase of the one-dimensional β-MnO_2 nanostructures using the direct reaction route is still challenging.

In this paper, we report a facile in-situ redox precipitation hydrothermal synthesis method for the selected control synthesis of single-crystal β-MnO_2 nanorods. The effects of various experimental conditions on the morphology and particle size of the products were studied. The mechanism of formation of the nanorods was investigated and discussed. The magnetic properties of the as-obtained nanorods with diameters of 25–40 nm and lengths of 240–440 nm were characterized.

2. Results and Discussion

2.1. Characterization

X-ray powder diffraction (XRD) patterns reveal the phase and purity of the as-obtained products. As shown in Figure 1, all of the reflection peaks can be indexed to a pure tetragonal phase of β-MnO_2 [JCPDS 24-0735, space group $P4_2/mnm$(136)] with lattice constants a = 4.3998 Å and c = 2.8695 Å. The sharp peaks indicate that the product is perfectly crystallized. No other impurity peaks were observed, demonstrating the high purity of the products obtained under current experimental conditions.

A typical TEM image of the as-prepared sample is shown in Figure 2 (a), which indicates that the final product consists of nanorods with diameters of 25–40 nm and lengths ranging from 240 to 440 nm. More detailed structural information for these nanorods was obtained from

[a] College of Chemistry, Chemical Engineering and Materials Science, Shandong Normal University,
Jinan, Shandong 250014, P. R. China
Fax: +86-531-86180017
E-mail: tangb@sdnu.edu.cn

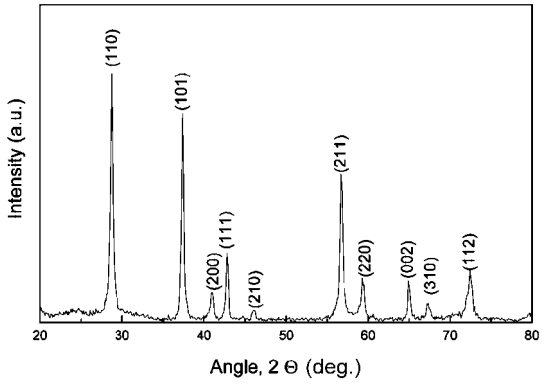

Figure 1. XRD pattern of the as-obtained product.

high-resolution transmission electron microscopy (HRTEM) images and selected area diffraction (SAED) patterns. The HRTEM image (Figure 2, b) of an individual nanorod shows that the nanorod is structurally uniform with an interplanar spacing of about 0.315 nm, which corresponds to the (110) plane of tetragonal β-MnO_2. Selected area electron diffraction patterns taken from the individual nanorod (shown in the inset image in Figure 2, b) reveal its single crystal nature, and can be indexed to the [001] zone axis of tetragonal β-MnO_2.

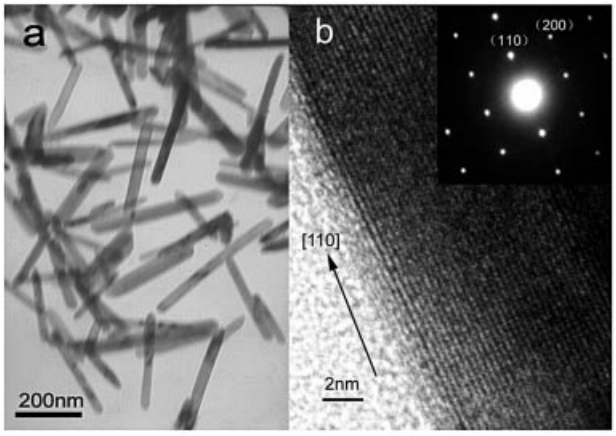

Figure 2. The (a) TEM image and (b) HRTEM and SAED (inset image) patterns of the as-prepared sample.

A typical room temperature X-ray photoelectron spectrum of the as-synthesized sample is shown in Figure 3. Only the peaks of Mn(2p3/2, 2p1/2) and O1s can be observed. The binding energies of Mn(2p3/2) and Mn(2p1/2) are 642.32 and 653.95 ev, respectively, which are well in accordance with MnO_2 [Mn(2p3/2) = 642.1 ev and Mn(2p1/2) = 653.8 ev].[25] The estimated relative ratio of O to Mn is 2.16:1, which is caused by the interference of oxygen in the air for the XPS study.

2. 2. The Effect of Reaction Conditions on the Morphology and Particle Size of the Products

2. 2. 1. The Effects of Ammonia on the Morphology and Particle Size of the Products

It was found that the concentration of ammonia as well as the way the ammonia was added had significant effects on the morphology of the products. Uniform nanorods were obtained (as shown in Figure 2, a) when ammonia was added dropwise. Pouring ammonia into the mixture of $Mn(NO_3)$ and H_2O_2 led to the product being composed of big rod-like structures (200–400 nm in diameter and more than 10 μm in length) and nanoparticles (Figure 4, a). The concentration of ammonia also significantly affected the morphology of the products. In our synthetic system, the concentrations of $Mn(NO_3)_2$ and H_2O_2 were kept constant and ammonia was added dropwise with different concentrations. As the concentration of ammonia was varied (0.25, 0.5, 1, 2 M) the morphology changed from a spindle morphology (Figure 4, b), to nanorods (Figure 2, a), a mixture of nanorods and nanoparticles (Figure 4, c), and finally to nanoparticles (Figure 4, d). From the above results, we can see that the precipitator ammonia in our synthetic system has significant effects on the morphology of the products.

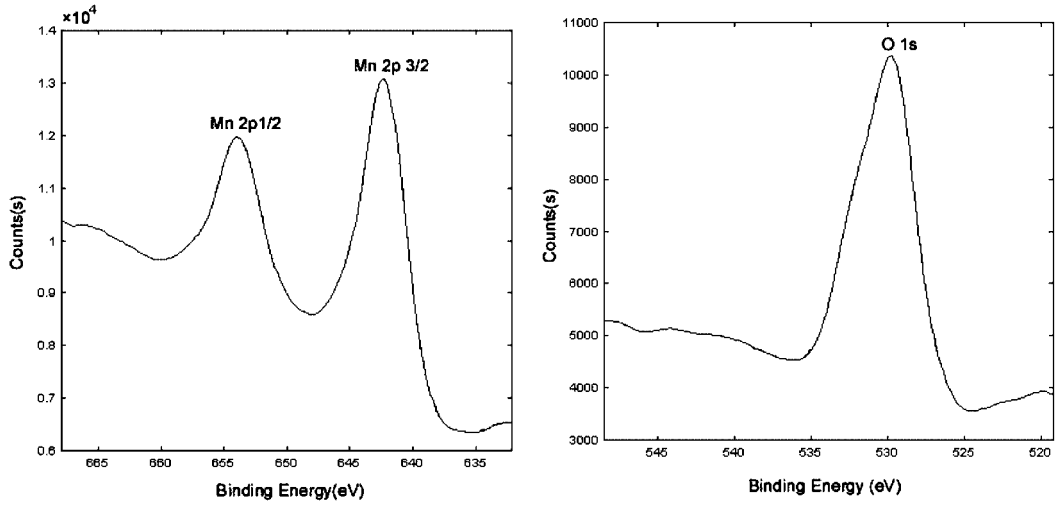

Figure 3. Room temperature X-ray photoelectron spectra of the as-obtained sample.

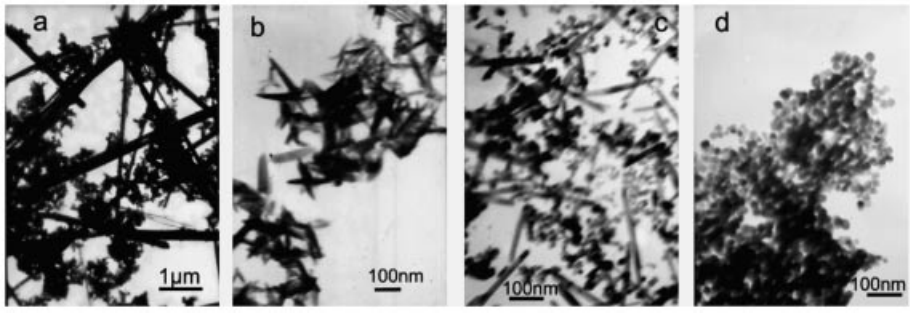

Figure 4. (a) 0.5 M ammonia was added by pouring, (b–d) ammonia was added dropwise with different concentrations; (b) 0.25 M; (c) 1 M; (d) 2 M.

2.2.2. Effects of H_2O_2 on the Morphology of the Products

Increasing the amount of H_2O_2 to 2 mL, while the other experimental conditions were kept constant, led to a morphology of the products similar to that shown in Figure 4 (a). The as-obtained products are composed of rod-like structures (400–500 nm in diameter and 10–20 μm in length) and nanoparticles.

2.2.3. Effects of Temperature on the Morphology of the Products

Temperature also affected the morphology and particle size of the final products. At a lower temperature such as 130 °C, only nanoparticles could be obtained (Figure 5, a). Upon increasing the temperature to 140 °C, we obtained a mixture of nanoparticles and nanorods (Figure 5, b). Nanorods could be obtained in the temperature range 180–250 °C. The TEM image in part c of Figure 5 shows that MnO_2 obtained at 180 °C consists of uniform nanorods with a diameter of 15–30 nm and lengths of 150–200 nm, whereas the product obtained at 210 °C is on average 20–30 nm in diameter and has a length of 200–300 nm as shown in part d of Figure 5. Upon increasing the temperature to 250 °C, the product was found to consist of uniform nanorods with a diameter of 25–40 nm and lengths of up to 240–440 nm as shown in Figure 2 (a). From the above results, we can see that the diameter and length of the nanorods increase slightly with increasing temperature. It is apparent that higher temperatures favor the anisotropic growth of the crystals and nanorod formation.

The phases of nanorods obtained in the temperature range 180–250 °C were examined by the X-ray powder diffraction technique, which demonstrated that all the phases were pure β-MnO_2. In contrast to solution-based methods for the growth of one-dimensional nanostructures in which the problem of phase control of the products often exists,[22] the present synthetic process can be performed over a wide range of hydrothermal reaction temperatures.

2.3. Possible Growth Mechanism of the Nanorods

The chemical reaction can be formulated as:

$$Mn^{2+} + H_2O_2 + 2\ NH_3{\cdot}H_2O \rightarrow MnO_2{\cdot}xH_2O + 2\ NH_4^+ + H_2O \quad (1)$$

$$MnO_2{\cdot}xH_2O \xrightarrow[\text{reaction}]{\text{hydrothermal}} MnO_2 + x\ H_2O \quad (2)$$

As illustrated in the chemical equation above, when ammonia was added to the mixture of hydrogen peroxide and manganese nitrate, the precipitation and oxidation reaction occurred together [Equation (1)], accompanied by the decomposition of hydrogen peroxide. After the in-situ redox precipitation process, we obtained $MnO_2{\cdot}xH_2O$. In the hydrothermal process, $MnO_2{\cdot}xH_2O$ dehydrated to MnO_2 [Equation (2)]. In order to investigate the growth process of

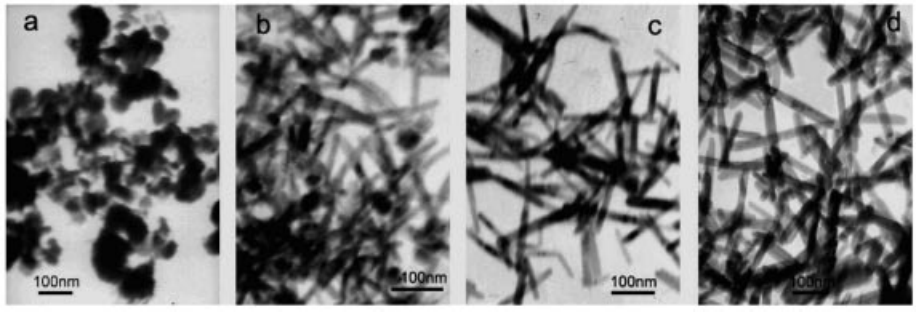

Figure 5. The products obtained at different hydrothermal reaction temperatures for 12 h: (a) 130 °C; (b) 140 °C; (c) 180 °C; (d) 210 °C.

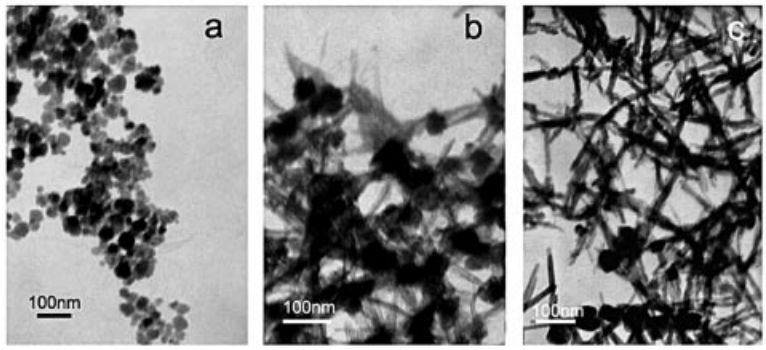

Figure 6. TEM image of the as-obtained samples at different hydrothermal reaction times: (a) 5 min; (b) 15 min; (c) 1 h.

the nanorods, we carried out the hydrothermal reaction at 250 °C for different periods of time. Figure 6 (a) shows the TEM image of the sample obtained after heating for 5 min, there are only nanoparticles with a diameter of 15–60 nm. The sample was characterized by XRD, but no peak was detected, indicting that crystallization did not occur for these nanoparticles. Figure 6 (b) shows the samples obtained after heating for 15 min, which indicates that there are nanoparticles with diameters of 40–60 nm and a few short nanorods. The smaller nanoparticles in Figure 6 (a) are not seen in Figure 6 (b). After heating for 1 h, the amount of nanorods is more than that shown in Figure 6 (b), and the amount of nanoparticles has dramatically decreased (Figure 6, c). The TEM image of the product obtained after heating for 12 h indicates that the product is composed of nanorods and the nanoparticles are no longer seen (Figure 2, a). The above study demonstrates that the nanorods are grown from the small nanoparticles. We believe that the mechanism of formation of the MnO_2 nanorods follows the Ostwald ripening process.[26]

3. Magnetic Property of the As-Synthesized β-MnO_2 Nanorods

The magnetic properties of the as-synthesized β-MnO_2 nanorods with a diameter of 25–40 nm and a length of 240–440 nm were characterized. Figure 7 shows the magnetization vs. temperature curve of the as-synthesized β-MnO_2 nanorods at an applied field of 1000 Oe. A kink is observed at 98 K in Figure 7, which corresponds to the Néel magnetic transition temperature T_N. This temperature is higher than that of the bulk MnO_2 crystal (T_N = 92 K),[27–28] which may be because of the special morphology and the effect of surface spins of the as-obtained nanorods.[29–30] Strangely, a discontinuity is seen in the temperature range 30–50 K in Figure 7. From the XRD and XPS studies, we know that the products we obtained were of high purity. So the reason for the discontinuity cannot be any impurity in the products, but may be caused by the special morphology and uncompensated surface spins of the nanorods.[29,31–32] At 293 K, a nearly linear M–H curve (Figure 8) reveals that a superparamagnetic state exists at this temperature.

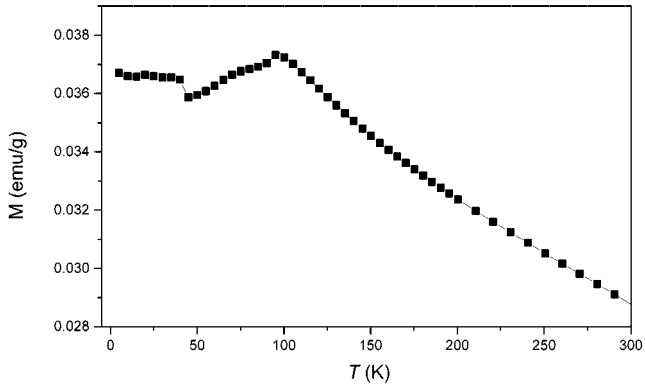

Figure 7. Magnetization vs. temperature curve of the as-obtained nanorods at an applied field of 1000 Oe.

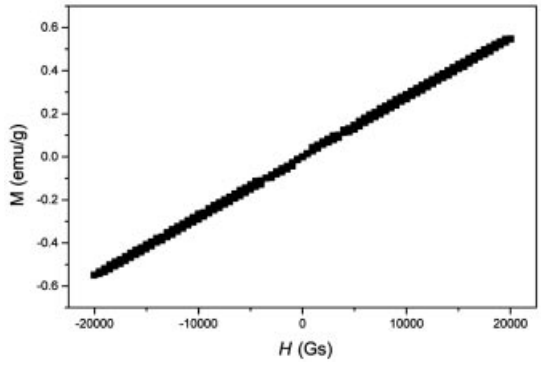

Figure 8. The magnetization vs. applied magnetic field of the as-obtained nanorods.

4. Conclusion

In summary, a simple in-situ redox precipitation hydrothermal synthesis method has been developed to synthesize single-crystal β-MnO_2 nanorods. The reactant ammonia and peroxide hydrogen as well as the hydrothermal reaction temperatures can greatly influence the morphology of the final products. Compared to the previous solution-based methods for the growth of 1D nanostructures in which the problem of phase control of products often exists, the present synthetic process can be performed over a wide range of hydrothermal temperatures. The magnetic measurements

indicate that the Néel temperature of the as-synthesized β-MnO_2 single crystals is about 98 K, which is about 6 K higher than that of the bulk β-MnO_2 crystals. The nanorod materials produced also may show possible novel electronic and catalytic properties induced by their dimensionality.

Experimental Section

MnO_2 nanorods were obtained by an in-situ redox precipitation hydrothermal synthesis method. In a typical experiment, hydrogen peroxide (1 mL, 30%) was added to an aqueous solution of manganese nitrate (12 mL, 0.3 mol/L) whilst stirring to form a homogeneous solution, then ammonia (5 mL, 0.5 mol/L) was added to the mixture dropwise. Upon the addition of ammonia, the precipitation of Mn^{2+} by ammonia to $Mn(OH)_2$ and the oxidization of $Mn(OH)_2$ by H_2O_2 were achieved immediately accompanied by the decomposition of H_2O_2. A brown suspension of $MnO_2{\cdot}xH_2O$ precipitated during the in-situ redox precipitation reaction. The resulting suspension was transferred into a 20-mL Teflon-lined autoclave up to 80% of the total volume. The sealed autoclave was heated at 250 °C for 12 h. The resulting black solid product was collected, washed several times with distilled water and absolute ethanol, centrifuged, and dried under vacuum at 60 °C for 3 h.

The phase and purity of the products were identified using X-ray powder diffraction (XRD) patterns collected with a Japan Rigaku Dmax-γA X-ray diffractometer with Cu-K_α radiation (λ = 1.54178 Å). A scan rate of 4°/min was applied to record the patterns in the 2θ range from 10 to 80°.The morphology and particle size of the products were determined with a Hitachi Model H-800 transmission electron microscope (TEM) operated at 200 kv. Structural information for the nanocrystals was obtained from selected area diffraction (SAED) patterns and high-resolution transmission electron microscopy (HRTEM) images obtained using a JEOL-2010F transmission electron microscope at an acceleration voltage of 200 kv. Electron diffraction patterns were obtained from samples during HRTEM measurements. X-ray photoelectron spectra were collected with a PHI5300 model XPS spectrometer with an Al-K_α radiation source. Magnetic properties were investigated with a superconducting quantum interference device (SQUID) magnetometer (MPMS-7).

Acknowledgments

This work was supported by the Program for New Century Excellent Talents in University (NCET-04-0651), the National Natural Science Foundation of China (Nos. 90401019 and 20335030) and the Excellent Young and Middle-aged Scientist Foundation of Shandong Province in China (No. 2004BS04002).

[1] W. U. Huynh, J. J. Dittmer, A. P. Alivisatos, *Science* **2002**, *295*, 2425–2427.
[2] Y. Xia, P. Yang, Y. Sun, Y. Wu, B. Mayers, B. Gates, Y. Yin, F. Kim, H. Yan, *Adv. Mater.* **2003**, *15*, 353–389.
[3] J. Wang, Q. W. Chen, B. Y. Hou, Z. M. Peng, *Eur. J. Inorg. Chem.* **2004**, 1165–1168.
[4] S. W. Chung, J. Y. Yu, J. R. Heath, *Appl. Phys. Lett.* **2000**, *76*, 2068–2070.
[5] N. R. Jana, L. Gearheart, C. J. Murphy, *Chem. Commun.* **2001**, 617–618.
[6] Y. Y. Wu, H. Q. Yan, M. Huang, B. Messer, J. H. Song, P. D. Yang, *Chem. Eur. J.* **2002**, *8*, 1260–1268.
[7] A. B. Panda, S. Acharya, S. Efrima, *Adv. Mater.* **2005**, *17*, 2471–2474.
[8] M. M. Thackeray, *Prog. Solid State Chem.* **1997**, *25*, 1–71.
[9] B. Ammundsen, J. Paulsen, *Adv. Mater.* **2001**, *13*, 493–496.
[10] L. Hueso, N. Mathur, *Nature* **2004**, *427*, 301–302.
[11] A. R. Armstrong, P. G. Bruce, *Nature* **1996**, *381*, 499–500.
[12] Q. Feng, H. Kanoh, K. Ooj, *J. Mater. Chem.* **1999**, *9*, 319–334.
[13] S. Bach, M. Henry, N. Baffer, J. Livage, *J. Solid State Chem.* **1990**, *88*, 325–333.
[14] J. T. Hu, T. W. Odom, C. M. Lieber, *Acc. Chem. Res.* **1999**, *32*, 435–445.
[15] M. H. Huang, S. Mao, H. Feick, H. Q. Yan, Y. Y. Wu, H. Kind, E. Weber, R. Russo, P. D. Yang, *Science* **2001**, *292*, 1897–1899.
[16] H. Kawamura, *J. Appl. Phys.* **1988**, *63*, 3086–3088.
[17] H. Sato, K. Wakiya, T. Enoki, T. Kiyama, Y. Wakabayashi, H. Nakao, Y. Murakami, *J. Phys. Soc. Jpn.* **2001**,*70*, 37–40.
[18] N. Yamamoto, T. Endo, M. Shimada, T. Takada, *Jap. J. Appl. Phys.* **1974**, *13*, 723–725.
[19] A. Yoshinori, *J. Phys. Soc. Jpn.* **1959**, *14*, 807–821.
[20] J. E. Greedan, N. P. Raju, A. S. Wills, C. Morin, S. M. Shaw, *Chem. Mater.* **1998**, *10*, 3058–3067.
[21] a) D. C. Golden, C. C. Chen, J. B. Dixon, *Science* **1986**, *231*, 717–718; b) R. N. DeGuzman, Y. F. Shen, E. J. Neth, S. L. Suib, C. L. young, S. Levine, J. M. Newsam, *Chem. Mater.* **1994**, *6*, 815–821; c) Y. F. Shen, R. P. Zerger, S. L. Suib, L. McCurdy, D. I. Potter, C. L. young, *Science* **1993**, *260*, 511–515; d) X. Wang, Y. D. Li, *Chem. Commun.* **2002**, 764–765; e) N. Kijima, H. Yasuda, T. Sato, Y. Yoshimura, *J. Solid State Chem.* **2001**, *159*, 94–102.
[22] X. Wang, Y. D. Li, *J. Am. Chem. Soc.* **2002**, *124*, 2880–2881.
[23] a) Y. Xiong, Y. Xie, Z. Li, C. Wu, *Chem. Eur. J.* **2003**, *9*, 1645–1651; b) Z. Y. Yuan, Z. L. Zhang, G. Du, T. Ren, B. Su, *Chem. Phys. Lett.* **2003**, *378*, 349–353.
[24] F. A. Al-Sagheer, M. I. Zaki, *Colloids Surf. A* **2000**, *173*, 193–203.
[25] J. Chastain, *Handbook of X-ray Photoelectron Spectroscopy*, 2nd ed., Perkin–Elmer Corporation, Wellesley, MA, **1992**, p. 79.
[26] A. R. Roosen, W. C. Carter, *Phys. A* **1998**, *261*, 232–247.
[27] A. Yoshinori, *J. Phys. Soc. Jpn.* **1959**, *14*, 807–821.
[28] N. Ohama, Y. Hamaguchi, *J. Phys. Soc. Jpn.* **1971**, *30*, 1311–1318.
[29] J. Park, E. Kang, C. J. Bac, J. G. Park, H. J. Noh, J. Y. Kim, J. H. Park, M. P. Park, T. Hyeon, *J. Phys. Chem. B* **2004**, *108*, 13594–13598.
[30] K. Woo, H. J. Lee, *J. Magn. Magn. Mater.* **2004**, *272–276*, 1155–1158.
[31] G. H. Lee, S. H. Huh, J. W. Jeong, B. J. Choi, S. H. Kim, H. C. Ri, *J. Am. Chem. Soc.* **2002**, *124*, 12094–12095.
[32] W. S. Seo, H. H. Jo, K. Lee, B. Kim, S. J. Oh, T. Park, *Angew. Chem. Int. Ed.* **2004**, *43*, 1115–1117.

Received: November 4, 2005
Published Online: March 30, 2006

